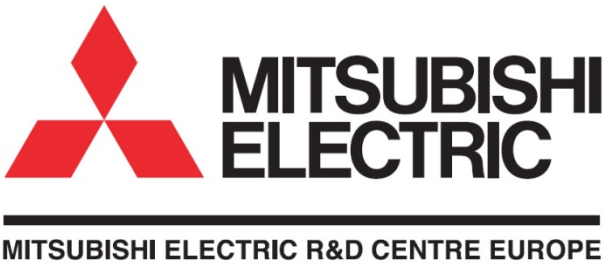

42nd Annual Conference of the IEEE Industrial Electronics Society (IECON) , Oct. 2016

DOI: 10.1109/IECON.2016.7793633

Real-life vs. standard driving cycles and implications on EV power electronic reliability

N. Degrenne
S. Mollov

Real-life vs. Standard Driving Cycles and Implications on EV Power Electronic Reliability

Synthesis of a Drive Cycle for Power Electronics Reliability Assessement

N. Degrenne, S. Mollov
Power Electronic System division
Mitsubishi Electric R&D Centre Europe (MERCE)
Rennes, France
n.degrenne@fr.merce.mee.com

***Abstract*— This work studies the impact of drive cycles on the power semiconductor temperature, and consequently on the reliability figures. The paper quantifies the reliability errors stemming from the use of standard mission profiles by comparing them to data sets using real-life high-resolution mission profiles. It is found that standard drive cycles under-estimate the stress on the power semiconductors. The paper thus proposes a new and more realistic Drive Cycle for Reliability Assessment (DCRA) to be used for lifetime estimation of power electronic components.**

Keywords—power semiconductor; automotive power converter; design for reliability; drive cycle; mission profile

I. INTRODUCTION

The reliability of power semiconductor modules was identified in [1] of major importance because: 1) most reported failures on power converters concern power semiconductors, 2) novel reliability critical applications such as automotive and wind energy emerge, and 3) novel component wide band gap devices and packaging technologies, for which failure modes are not known, start penetrating the market.

Design for reliability consists in designing a power semiconductor module not only with respect to functional requirements but also to reliability and robustness requirements [2-4]. It necessitates estimating lifetime of the module under study, usually with minimum reliability figure in mind.

Recently, the lifetime estimation is obtained with a stepwise approach [5-6] from an estimation of the usage (mission profile). The process employs an electrical, thermal and damage model of the Device Under Test (DUT) (Fig. 1). This approach assumes that the device will be used according to the pre-defined and representative mission profile.

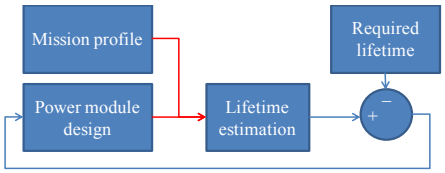

Figure 1. Design for reliability

This paper studies the influence of realistic mission profiles on the thermo-mechanical stress in a power semiconductor module used for the traction of an Electric Vehicle (EV), and has no convocation of proposing a new test cycle. First, typical speed profiles are presented. Then, a method is described to convert the speed profiles into histograms of thermo-mechanical stressors. Next, the stressors generated by the different speed profiles are discussed. Finally, a new, more representative speed profile is proposed.

II. SPEED PROFILES

A collection of drive cycles corresponding to different types of driving is available in the literature [7]. At present, the New European Driving Cycle (NEDC) in Fig. 2 is generally accepted as a profile that represents well a typical driving style. For example, it is used in [8] to optimize the design of modular converters. It is also used in [9-10] to assess the reliability of power semiconductor devices. This profile was last updated in 1997 to assess the emission levels of car engines and fuel consumption in passenger cars. Thus, the legitimacy of the NEDC to assess the reliability of power semiconductor modules is questionable; particularly since the Worldwide harmonized Light vehicles Test Procedures (WLTP) in Fig. 2 defined in 2015 a set of speed profiles to replace the NEDC.

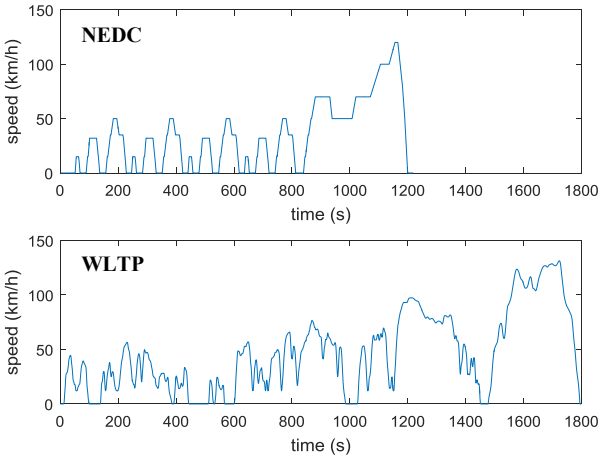

Figure 2. Standard drive cycles

Although more realistic than the NEDC, the WLTP profiles are considered to be slow. For example, the time of the most rapid acceleration between 0 and 50km/h is 15seconds, which is considered unrealistically slow. This is why, this paper compares the NEDC and the WLTP profiles to a speed profile derived from high-resolution data on real drive cycles. This high-resolution data consists of 154 drives cycles totalizing 50h and 565km driven by 5 different drivers on a Renault Kadjar with 130hp. Speed was monitored every 0.1s using an On Board Diagnostic (OBD) link that reads a speed value in km/h with a two digit resolution.

III. GENERATION OF STRESS HISTOGRAMS AND DAMAGE LEVELS

This section presents a methodology that evaluates the level of damage caused on a traction power semiconductor device when an EV is subject to a particular drive cycle.

A. Electromechanical model

The objective of the electromechanical model is to convert the speed profile into a load current provided by the motor drive. This model is useful when no data from current/voltage sensors is directly available. First, the mechanical force (N) is derived using (1):

$$F = m \cdot a + 0.5 \cdot Cx \cdot \rho \cdot S \cdot v^2 + m \cdot g \cdot Kr \tag{1}$$

where m is the mass (1568kg), a is the acceleration ($m.s^{-2}$) derived from the speed v ($m.s^{-1}$) with a minimum value clamped at $-2 m.s^{-2}$, Cx is the drag coefficient (0.338), ρ is the mass density of air ($1.204 kg.m^{-3}$), S is the reference area ($2.22 m^2$), g is the local acceleration ($9.8 N.kg^{-1}$), and Kr is the rolling factor (0.012). This data set was inspired by Renault Zoe characteristics. Equation (1) assumes that the car is driven on a flat road and that all the parameters are constant. Then, the electrical power is derived using (2):

$$Pelec = abs(F) \cdot v / \eta \tag{2}$$

where η is the transmission and motor efficiency (0.75). Next, the phase to phase rms voltage $Urms$ is defined taking a simple assumption of linearity dependency with car speed (3):

$$Urms = \frac{\sqrt{3}}{2\sqrt{2}} \cdot (A \cdot v + B) \cdot Vdc \tag{3}$$

where A ($0.0266 s.m^{-1}$) and B (0.011) are constants defining the modulation index with the assumption that the maximum speed is 140km/h, and Vdc is the DC-bus (i.e. battery) voltage (400V). After that, the phase current $Irms$ is computed using (4):

$$Irms = Pelec / (Urms * \cos(\varphi) * \sqrt{3}) \tag{4}$$

where $cos(\varphi)$ is the power factor (0.8). The outputs of the electromechanical model are illustrated in Fig. 3 for NEDC and WLTP standard drive cycles.

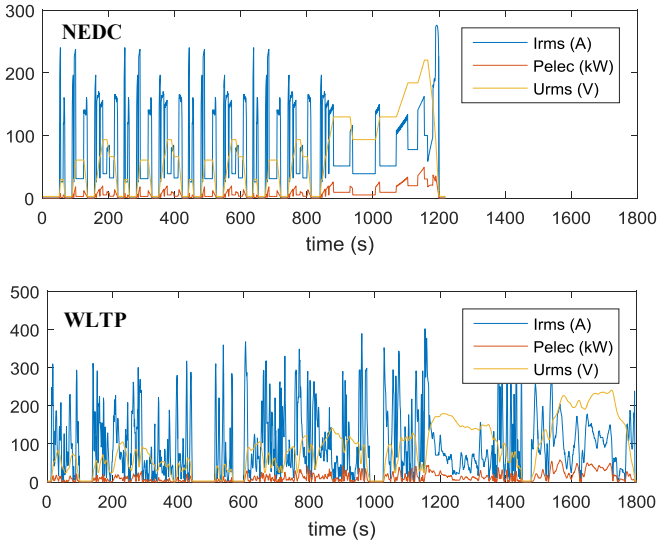

Figure 3. Outputs of the electromechanical model with NEDC (top) and WLTP (bottom) standard drive cycles

B. Power loss model

The objective of the power loss model is to compute the losses in the IGBT and diodes of a 3-phase motor drive. The method uses conduction and switching characteristic that can be found in the datasheets of commercially available modules. The average conduction losses in the IGBTs Pcd_igbt and diodes Pcd_diode are expressed using equations (5) and (6) [11]:

$$\begin{aligned} Pcd\_igbt &= 0.5 \cdot \left(Vt \frac{\sqrt{2} \cdot Irms}{\pi} + Rt \frac{Irms^2}{2}\right) \\ &+ sg(a) \cdot (A \cdot v + B) \cdot \cos(\varphi) \cdot \left(Vt \frac{\sqrt{2} \cdot Irms}{8} + Rt \frac{2 \cdot Irms^2}{3\pi}\right) \end{aligned} \tag{5}$$

$$\begin{aligned} Pcd\_diode &= 0.5 \cdot \left(Vd \frac{\sqrt{2} \cdot Irms}{\pi} + Rd \frac{Irms^2}{2}\right) \\ &- sg(a) \cdot (A \cdot v + B) \cdot \cos(\varphi) \cdot \left(Vd \frac{\sqrt{2} \cdot Irms}{8} + Rd \frac{2 \cdot Irms^2}{3\pi}\right) \end{aligned} \tag{6}$$

where Vt, Rt, Vd and Rd represent the constant and current-dependent voltage drop across the IGBT and diode during ON-state. The sign of the power factor equals the sign of the acceleration $sg(a)$. The average switching losses in the IGBTs and diodes are expressed using equations (7) and (8):

$$Psw\_igbt = \frac{f}{\pi} \cdot (Eton + Etoff) \cdot \frac{Vdc}{Vtref} \cdot \frac{Irms}{Itref} \tag{7}$$

$$Psw\_diode = \frac{f}{\pi} \cdot (Edon + Edoff) \cdot \frac{Vdc}{Vdref} \cdot \frac{Irms}{Idref} \qquad (8)$$

where *Eton*, *Etoff*, *Edon* and *Edoff* are the energy losses (J) in the IGBT and diode during ON and OFF commutations. They are provided by the datasheet at reference voltages and currents *Vtref*, *Itref*, *Vdref* and *Idref*, and are therefore scaled linearly according to the actual *Vdc* and *Irms* values.

The power loss model outputs the instantaneous power losses in the 6 IGBTs and the 6 diodes of the 3-phase inverter. This inverter can for example be implemented with three 650V/600A EconoDUAL3 modules (ref FF600R07ME4_B11) from Infineon. Figure 4 was generated with the parameters of this module.

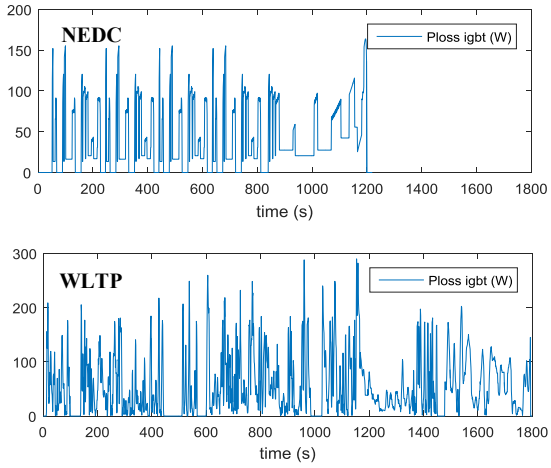

Figure 4. Outputs of the power loss model computed with FF600R07ME4_B11 power module with NEDC (top) and WLTP (bottom) standard drive cycles

C. *Thermal model*

The objective of the thermal model is to compute the temperature of the IGBT and diode dies. The thermal model can be considered as a transfer function which inputs are the losses in the IGBTs and diodes, and outputs are the junction temperatures of the IGBTs and diodes.

The thermal behavior within the power modules (i.e. from junction to case) is provided in the datasheet in the form of two Foster models, one for the IGBTs and one for the diodes. The Foster models are useful for determining the junction temperature when the case temperature is known. In order to estimate the case temperature of the modules, the Foster models are approximated by a 1-layer Cauer model. The power out of 1-layer Cauer models are summed and used as an input for a Cauer model representing the thermal behavior of the grease ($0.01K.W^{-1}$) and the heat-sink ($1102J.K^{-1}$ and $0.015K.W^{-1}$). Each module is supposed to be mounted on an independent heat-sink, and the ambient temperature *Tamb* is assumed to be constant and equal to 25°C. The block diagram, adapted from [12] is summarized in Fig 5. As a result, Fig. 6 provides the estimation for the junction, case, and heat-sink for NEDC and WLTP drive cycles. It can be observed that the temperature cycles have higher amplitude and are more numerous for the WLTP drive cycle.

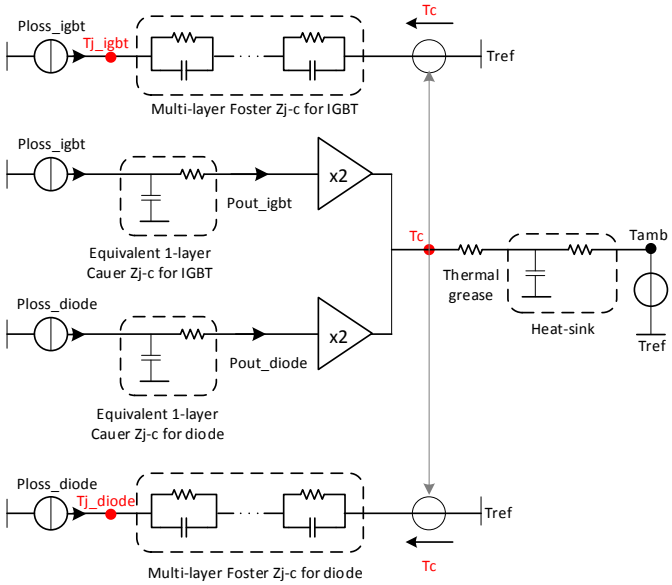

Figure 5. Thermal model block diagram adapted from [12]

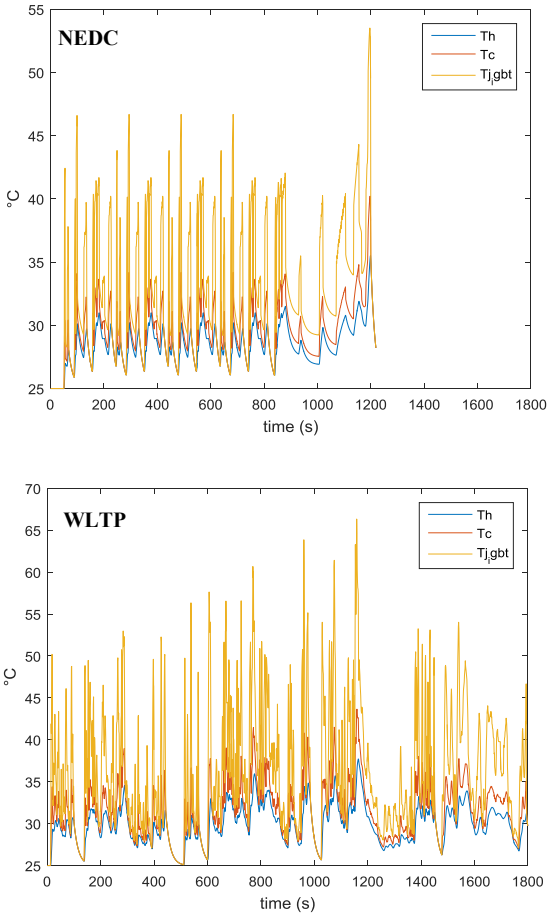

Figure 6. Estimated temperature profiles for the NEDC (top) and WLTP (bottom) standard profiles

D. Temperature cycle counting

The objective of the temperature cycle counting stage is to generate a histogram with 3-dimensions representing respectively temperature variation, mean temperature, and cycle count.

The rainflow algorithm is used because it provides overall best performances when compared to other algorithms [13]. The algorithm was implemented on Matlab. Temperature histograms generated for NEDC and WLTP are shown in Fig. 7. The histograms confirm the presence of temperature cycles with higher amplitude and mean values for the WLTP drive cycle.

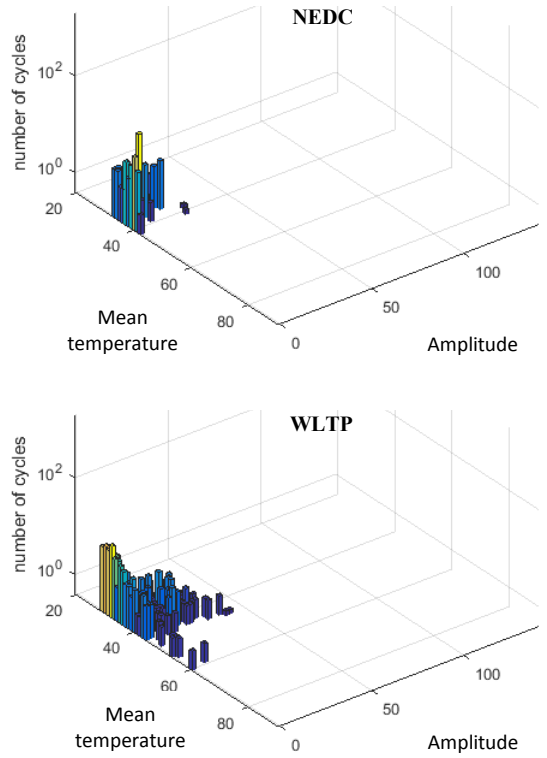

Figure 7. Temperature histograms generated by the rainflow algorithm for the NEDC (top) and WLTP (bottom) standard profiles

E. Damage estimation

The objective of this last stage is to estimate the level of damage caused by the temperature cycles during the drive cycle. Indeed, thermo-mechanical stress is accumulated in the power module assembly. This is caused by thermal expansion mismatches caused by CTE mismatches and thermal gradients. Some power cycling tests correlate the number of cycle to failure to the temperature variations and mean temperatures of the dies. The LESIT life law [14] is one of the well accepted relations and it fits with the available data format as, unlike the CIPS model, it does not depend on heating time. It also better fits the reliability figures of current modules at the applicable temperature ranges. It is composed of a Coffin-Manson and an Arrhenius term (9):

$$Nf = C \cdot \Delta T_j^{\alpha} \cdot \exp\left(\frac{E_a}{k_B \cdot T_m}\right) \quad (9)$$

where k_B is the Boltzmann constant ($1.38\text{x}10^{-23}\text{J.K}^{-1}$), Ea ($9.89\text{x}10^{-20}$J), C ($302500\text{K}^{-\alpha}$) and α (-5.039) are typical parameters given in [15].

With this equation, each temperature cycle that was identified and classified by the rainflow algorithm is related to a damage level $1/Nf$. The damages of all the individual temperature cycles are summed with the assumption of the Miner linear damage accumulation.

IV. Comparison of Driving Cycles

The methodology described above to estimate the stress histograms and damage levels relies on a large number of assumptions that can be discussed. This is why it only provides a tool to perform a relative comparison of standard drive cycles and high-resolution data consisting of 154 real drives cycles. The temperature histograms were derived for the real drive cycles performed by 5 employees of MERCE in Rennes, France. The global histogram summing the thermal cycles of all the logs is in Fig. 8. The reliability figures are summarized in Table 1 for the NEDC, the WLTP, and the real logs. The distance to failure provides the number of km performed under a particular drive profile before the accumulated damage reaches the value of one. When comparing the two standard drive cycles, large differences can already be seen. WLTP is a more stressful profile than NEDC (3.33 times shorter distance to failure). It has larger and more numerous temperature excursions attributed to faster and more accelerations and decelerations. The real logs are even more stressful (16.53 times shorter distance to failure than WLTP). This result tends to indicate that standard drive cycles are inappropriate to estimate the reliability of power semiconductor devices in EV applications. In order to allow fast design for reliability, a more realistic drive cycle is required.

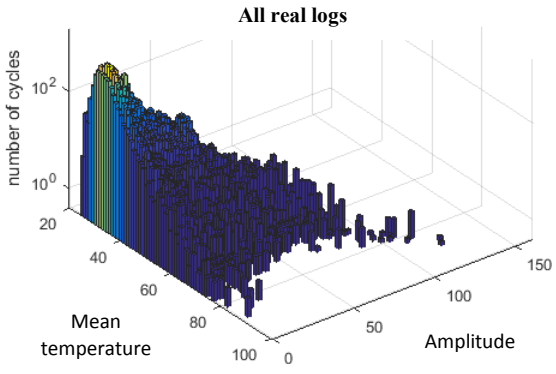

Figure 8. Temperature histogram generated by the rainflow algorithm for all the high-resolution real drive cycles.

Table 1: Comparison of NEDC, WLTP and real logs

Drive cycle	Maximum acceleration ($m.s^{-2}$)	Length(km)	Damage (1=failure)	Distance to failure (km)
NEDC	1.39	3.059	$0.57x10^{-6}$	**$5390x10^{3}$**
WLTP	1.75	6.462	$3.98x10^{-6}$	**$1620x10^{3}$**
Real logs	6.90	564.698	$3581x10^{-6}$	**$98x10^{3}$**

V. Generation of the Drive Cycle for Reliability Assessement (DCRA)

Figure 9 shows the speed and acceleration histograms for the WLTP and the real logs. From this figure, it is possible to see that the major difference between the WLTP and the real logs is the acceleration and not the speed. Thus, it was decided to build the new profile as an evolution of the WLTP standard profile where the accelerations are amplified while the speed plateaus are conserved.

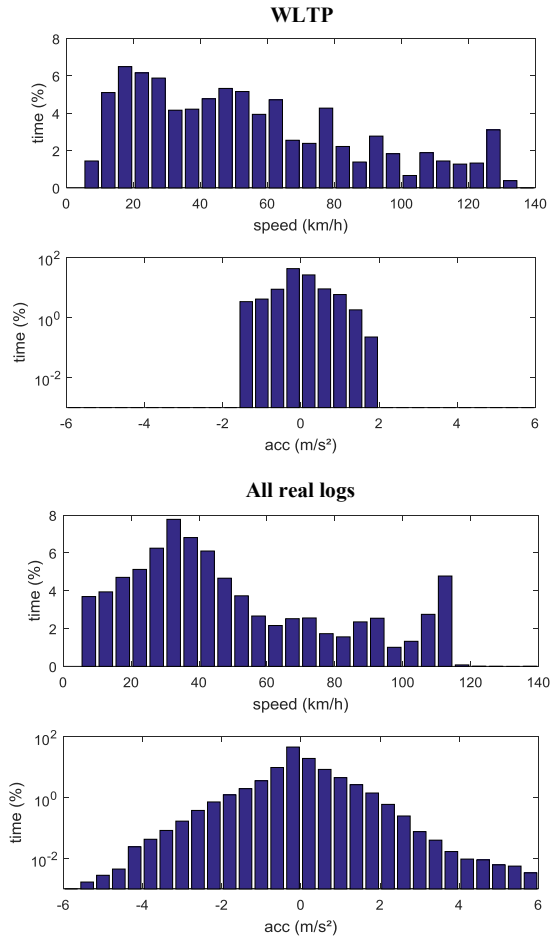

Figure 9. WLTP and real logs speed and acceleration histograms

In the original WLTP profile, the time step is 1s between each speed value. In order to generate the DCRA, the time step vector *tmstp* is modified according to (10):

$$tmstp = \frac{1}{D \cdot abs(a) + 1} \tag{10}$$

where D (0.413) is a scaling parameter that can be modified to tune the acceleration amplification factor. The time step vector is then scaled to conserve the same drive cycle duration as the original WLTP. The new time scale is generated by performing the cumulative sum of the time steps. Finally the speed vector is interpolated to produce a drive cycle with a final time step of 1s, as the original WLTP drive cycle. The synthesized DRCA is shown in Fig. 10. As can be seen, the DCRA is very similar to the WLTP, with a same duration and similar speed plateaus. Only the speed transients are amplified in the case of the DCRA. The corresponding acceleration profile is shown in Fig. 11. As can be seen, even if the speed plateaus are similar, the accelerations are amplified for the DCRA drive cycle. The temperature histogram of the DCRA in Fig. 12 shows cycles with higher mean and amplitude values than the temperature histogram of the WLTP. Finally, the DCRA mission profile was tested and is compared to the real-life data in Table 2. The distance to failure is similar because the scaling parameter D was defined with this objective in mind. The maximum acceleration is lower for the DCRA than with real logs because the DCRA is only a 30min, 6km (and therefore incomplete) representation of the real logs, with similar distance to failure.

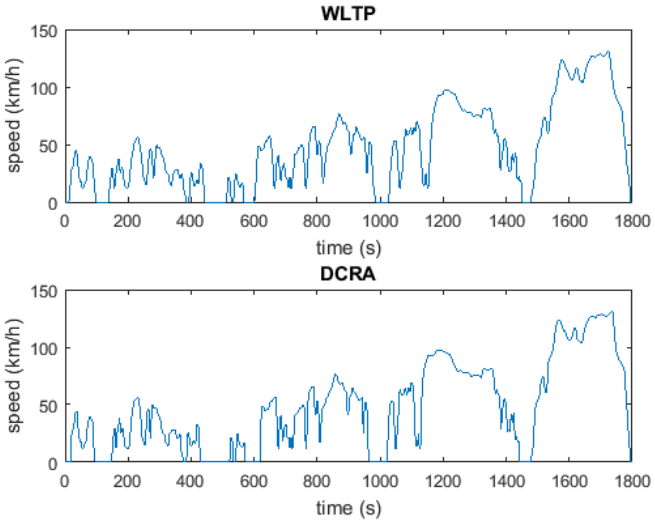

Figure 10. WLTP and DCRA speed drive cycles

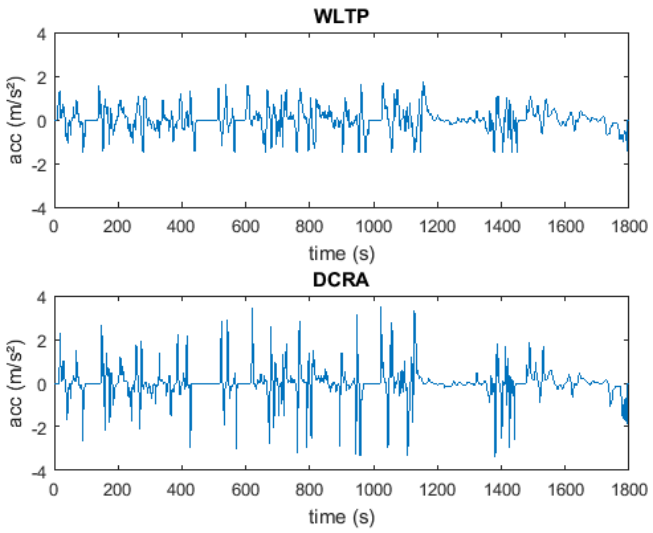

Figure 11. Acceleration for the WLTP and DCRA speed drive cycles

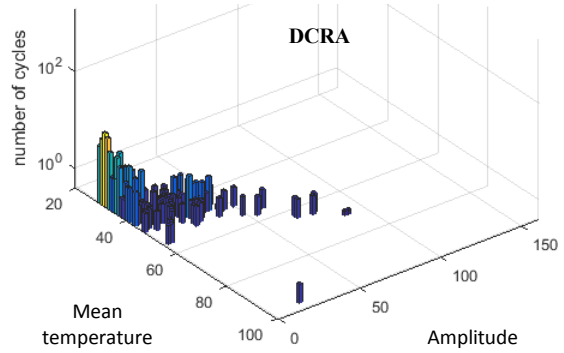

Figure 12. Temperature histogram generated by the rainflow algorithm for the DCRA drive cycle

Table 2: Comparison of real logs and DCRA

Drive cycle	**Maximum acceleration ($m.s^{-2}$)**	**Length(km)**	**Damage (1=failure)**	**Distance to failure (km)**
Real logs	6.90	564.698	$3581x10^{-6}$	**$98x10^3$**
DCRA	3.58	6.685	$66.85x10^{-6}$	**$98x10^3$**

VI. Conclusion

A methodology was presented to estimate the stress histograms and damage caused on a power semiconductor module by a drive cycle. The method was used to compare standard drive cycles (NEDC and WLTP) to real drive data. The standard drive cycles represent poorly the real operating conditions during driving. Finally, a new profile, so-called Drive Cycle for Reliability Assessment (DCRA) is synthesized, that more accurately represents realistic drive conditions. This new drive cycle can be used for reliability assessment of power semiconductor devices.

Acknowledgment

The authors thank Eric Lavillonnière and David Mottier from the Communication division of Mitsubishi Electric R&D Centre Europe for sharing drive data.

References

[1] N. Degrenne, J. Ewanchuk, E. David, R. Boldyrjew, S. Mollov, "A Review of Prognostics and Health Management for Power Semiconductor Modules," in PHM society conference 2015
[2] H. Lu, C. Bailey, and C. Yin, "Design for reliability of power electronics modules," Microelectron. Reliab., vol. 49, no. 9–11, pp. 1250–1255, Sep. 2009.
[3] ZVEI, "Handbook for Robustness Validation of Automotive Electrical / Electronic Modules," 2013.
[4] ZVEI, "Handbook for Robustness Validation of Semiconductor Devices in Automotive Applications," 2013.
[5] M. Thoben, K. Mainka, R. Bayerer, I. Graf, and M.Munzer, "From Vehicle Drive Cycle to Reliability Testing of Power Modules," Automot. Power, no. 6, pp. 6–9, 2008.
[6] D. Hirschmann, D. Tissen, S. Schröder, and R. W. De Doncker, "Reliability prediction for inverters in hybrid electrical vehicles," IEEE Trans. Power Electron., vol. 22, no. 6, pp. 2511–2517, 2007.
[7] T. Barlow, S. Latham, I. McCrae, and P. Boulter, A reference book of driving cycles for use in the measurement of road vehicle emissions. 2009.
[8] J. Biela, S. Waffler, and J. W. Kolar, "Mission profile optimized modularization of hybrid vehicle DC/DC converter systems," PEMC 2009, pp. 1390–1396, 2009.
[9] Y. Wang, S. Jones, a. Dai, and G. Liu, "Reliability enhancement by integrated liquid cooling in power IGBT modules for hybrid and electric vehicles," Microelectron. Reliab., Aug. 2014.
[10] P. James, "Health Monitoring of IGBTs in Automotive Power Converter Systems," PHD Thesis. University of Manchester, 2012.
[11] ABB, "Application Note 5SYA 2053-04: Applying IGBTs."
[12] K. Ma, Y. Yang, and F. Blaabjerg, "Transient modelling of loss and thermal dynamics in power semiconductor devices," Energy Convers. Congr. pp. 5495–5501, 2014.
[13] K. Mainka, M. Thoben, and O. Schilling, "Lifetime calculation for power modules, application and theory of models and counting methods," EPE 2011.
[14] M. Held, P. Jacob, G. Nicoletti, P. Scacco, and M.-H. Poech, "Fast power cycling test of IGBT modules in traction application," PEDS 1997.
[15] J. Lutz, H. Schlangenotto, U. Scheuermann, and R. De Doncker, Semiconductor power devices: Physics, characteristics, reliability. Springer, 2011.